Substrate Stiffness Increases Twitch Power of Neonatal Cardiomyocytes in Correlation with Changes in Myofibril Structure and Intracellular Calcium

Anthony G. Rodriguez,[†] Sangyoon J. Han,[‡] Michael Regnier,[†] and Nathan J. Sniadecki[†‡*]
[†]Department of Bioengineering and [‡]Department of Mechanical Engineering, University of Washington, Seattle, Washington

ABSTRACT   During neonatal development, there is an increase in myocardial stiffness that coincides with an increase in the contractility of the heart. In vitro assays have shown that substrate stiffness plays a role in regulating the twitch forces produced by immature cardiomyocytes. However, its effect on twitch power is unclear due to difficulties in measuring the twitch velocity of cardiomyocytes. Here, we introduce what we consider a novel approach to quantify twitch power by combining the temporal resolution of optical line scanning with the subcellular force resolution of micropost arrays. Using this approach, twitch power was found to be greater for cells cultured on stiffer posts, despite having lower twitch velocities. The increased power was attributed in part to improved myofibril structure (increased sarcomere length and Z-band width) and intracellular calcium levels. Immunofluorescent staining of α-actin revealed that cardiomyocytes had greater sarcomere length and Z-band width when cultured on stiffer arrays. Moreover, the concentration of intracellular calcium at rest and its rise with each twitch contraction was greater for cells on the stiffer posts. Altogether, these findings indicate that cardiomyocytes respond to substrate stiffness with biomechanical and biochemical changes that lead to an increase in cardiac contractility.

INTRODUCTION

During development, the elastic modulus of heart tissue increases threefold from embryonic to neonatal stages in mice (1) and doubles from neonatal to adult stages in rats (2). This stiffening of the myocardium coincides with an increase in the capacity of the heart to pump blood (3–5). At the cellular level during development, cardiomyocytes have improved contractility that is associated with a hypertrophic growth phase, leading to cells that are larger in size and that have increased myofibril density, alignment, and resting sarcomere length (4–6). These cells also exhibit a high degree of plasticity, enabling them to adapt to changes in their physical environment (7,8). Similar observations of myodifferentiation and myofibrillogenesis in response to substrate stiffness have been seen in satellite cells (9), mesenchymal stem cells (10), and other cardiac progenitors (11). Additionally, higher substrate stiffness can have a positive effect on intracellular calcium transients (12), which in turn increases cardiac contractility (13,14). These observations suggest that changes in myocardial stiffness after birth may help improve the contractile power of the cardiomyocytes by affecting a change in myofibril structure and performance.

Studying how cardiac contractility responds to changes in stiffness has been difficult due to the inability to measure twitch power. Others have used maximum twitch force as a metric of contractility and reported that cardiomyocytes produce more force in response to higher substrate stiffness (10,12,15–17). Although force is an important component of contractility, twitch power is a more complete metric because it reflects the heart's rate of work during the ejection phase of systole (18,19). However, measuring twitch power in response to stiffness requires improved cell culture assays with well-defined stiffnesses that allow for simultaneous measurement of twitch velocity and force. Because force and velocity are not constant throughout a twitch contraction, capturing the dynamics of a twitch requires a high degree of temporal resolution in the measurement approach. This limits the application of previous approaches that analyzed contractility in primarily isometric or isotonic conditions (14,18–21).

In this study, we developed what we consider a novel approach that combines high-speed line scanning with microfabricated arrays of flexible posts. This approach provided the temporal resolution necessary to measure the power of neonatal rat cardiomyocytes cultured on post arrays of different stiffness. The microposts acted as force sensors and line scanning was able to track the deflections of the posts at a frequency that was 20 times greater than video microscopy. Others have measured neonatal cardiomyocytes on arrays of posts previously (22–24), but without sufficient temporal resolution to assess twitch dynamics. Using our approach, cardiomyocytes were found to have a twitch power that was greater when cultured on substrates with higher stiffness. Cardiomyocytes on these stiffer arrays had greater sarcomere length and Z-band width, indicating that organization of myofibril structure was influenced by substrate stiffness. We further determined that intracellular calcium levels during a twitch contraction increased with stiffness, which matched with the higher twitch forces observed. Based on these findings, we propose that along with increased calcium activation, neonatal rat cardiomyocytes undergo structural improvements within their myofibril array in

response to the higher stiffness of their environment, resulting in a more powerful twitch contraction.

MATERIALS AND METHODS

Microposts

Polydimethylsiloxane (PDMS, Sylgard 184; Dow Corning, Midland, MI) was used to produce arrays of microposts on glass coverslips through a replica-molding process from silicon masters as previously reported (25). The thickness of the PDMS film underneath the microposts was 35 ± 5 μm. The spring constant of a post, k, was calculated by

$$k = \frac{3\pi E D^4}{64 L^3}, \tag{1}$$

where E is the Young's modulus of PDMS, D is the diameter, and L is height of the post. Four different arrays of microposts were used that had uniform spring constants of 29 ± 16, 76 ± 8, 103 ± 14, and 142 ± 30 nN/μm, as estimated from the dimension of the posts and tensile measurements of PDMS (26). These arrays had effective shear moduli of 3 ± 2, 8 ± 1, 10 ± 1, and 15 ± 2 kPa, based upon the spacing, diameter, and height of the microposts within the array (see Appendix). These shear moduli were chosen because they closely matched the stiffness measured in myocardial tissue during postnatal development (1,2,27). Arrays were prepared for cell culture by microcontact-printing fibronectin (50 μg/mL; BD Biosciences, Franklin Lakes, NJ) onto the tips of the posts. The arrays were then incubated in 0.2% Pluronics (Sigma-Aldrich, St. Louis, MO) overnight at 4°C to block the adsorption of additional proteins to the surface of the microposts.

Cell culture

Cardiomyocytes were isolated from 2- to 4-day-old newborn Fischer 344 rats, as previously described (27), under approval of the University of Washington Animal Care Committee and in accordance with federal guidelines. Before seeding, arrays were submerged in 2 mL of plating media at a 4:1 ratio of Dulbecco's modified Eagle's medium (DMEM; HyClone, Logan, UT) and M199 (10% horse serum, 5% fetal bovine serum, 20 mM HEPES, 100 U/mL penicillin G, 100 μg/mL streptomycin, and 4 mM glutamine). Harvested cells were resuspended in plating media at a density of 1000 cells/μL and transferred to the substrates in 200 μL aliquots for a total of 200,000 cells per substrate. Within 24 h of seeding, culture media was changed and supplemented with 10 μM arabinosylcytosine to remove proliferating cells (such as fibroblasts) in the culture. All reagents were purchased from Sigma-Aldrich unless specifically noted.

Measurement of force and work

After seeding, cardiomyocytes were cultured on micropost arrays for five days before measurements were made. This time under culture allowed the cells to adhere to posts, fully spread, and develop their myofibrils. The arrays with cells were placed into a field stimulation chamber (IonOptix, Milton, MA) with Tyrode's buffer (10 mM HEPES, 138 mM NaCl, 5.5 mM glucose, 12 mM NaHCO$_3$, 0.36 mM Na$_2$HPO$_4$, 2.9 mM KCl, 0.5 mM MgCl$_2$, and 1 mM CaCl$_2$ at pH 7.4). A stimulation field of 5 V and 0.5 Hz was applied to induce twitch contractions. Cardiomyocytes that contracted against the posts in response to the stimulation were recorded on a Ti-E microscope using a 40× objective (Nikon, Melville, NY) under phase-contrast and a cooled charge-coupled device camera (CoolSnap HQ^2; Photometrics, Tucson, AZ). Cells were not analyzed if they were in contact with adjacent cells, did not contract under stimulation, or failed to visibly deflect the posts. On average, the duration of time that posts were deflected for >90% of their maximum deflection was 190 $\pm$

20 ms. Consequently, using the Nyquist sampling theorem, a minimum of 10.5 fps was required to record the maximum deflection in a post from a twitch contraction.

A Gaussian fitting algorithm in IGOR (WaveMetrics, Lake Oswego, OR) was used to identify the position of each post in a frame, as previously described in Sniadecki et al. (28). From analysis of the videos, the deflection of a post, δ, during a twitch contraction was determined by

$$\delta = x_i - x_{ref}, \tag{2}$$

where x_i is the position of a post in the ith video frame during a twitch contraction and x_{ref} is its reference position taken a point in time between contractions, i.e., its resting state. The instantaneous twitch force, F, could be calculated for each frame in the video by

$$F = k\delta. \tag{3}$$

The force at a post that a cell produced during its resting state was calculated from the difference in its resting position (x_{ref}) and its original, undeflected position. The undeflected positions of the posts were found by determining the location of the intersections between best-fit lines through the rows and columns of nearby posts in the field of view that were not in contact with the cell. Additionally, the contractile work at a post, W, was estimated by the change in its strain energy, ΔU, during the shortening phase of the twitch contraction,

$$W = \Delta U = \frac{1}{2} k \left(x_i^2 - x_{ref}^2 \right). \tag{4}$$

Measurement of velocity and power

As previously described for video microscopy, cells were placed in an IonOptix field stimulation chamber, stimulated at 5 V and at 0.5 Hz. Posts at the perimeters of cells were measured with IonOptix's line scanning software and IonOptix optical equipment. Briefly, the image of a post was positioned in the field of view of the camera such that its deflection was aligned with the axis of the scan line (see Fig. 3 A). The leading edge of the post was represented by a local minimum in the light intensity profile and its position along the scan line was tracked throughout the twitch contraction. On average, the duration at which the velocity of a post was >90% of its maximum velocity was 16 $\pm$ 4 ms. Subsequently, using the Nyquist sampling theorem, a minimum of 154 Hz was required to record the absolute maximum velocity of a twitch contraction. In comparison, line scanning with IonOptix provided 240 Hz of temporal resolution, which was adequate to capture maximum velocity of a twitch.

The data collected were filtered with a Butterworth low-pass filter. Instantaneous velocity, v, was calculated by

$$v = \frac{d\delta}{dt} = \frac{(\delta_{i+1} - \delta_{i-1})}{(t_{i+t} - t_{i-1})}, \tag{5}$$

where i is the frame number and t is time. From Eqs. 2, 3, and 5, the instantaneous power, P, could be determined by

$$P = \frac{d}{dt}(F\delta) = F\frac{d\delta}{dt} + \delta\frac{dF}{dt} = F\frac{d\delta}{dt} + \delta\frac{d(k\delta)}{dt} = 2F\frac{d\delta}{dt}. \tag{6}$$

It should be noted that the first term is the conventional definition of power whereas the second term accounts for the fact that the loading rate of force on a post is not constant during a twitch contraction.

Measurement of intracellular calcium

Cardiomyocytes on the softest (3 kPa) and stiffest (15 kPa) arrays were loaded with 2 μM Fura-2 AM (Molecular Probes, Eugene, OR) in Tyrode's

buffer and measured with the IonOptix system for intracellular calcium analysis. The ratio of fluorescent intensities between wavelengths of 360 nm and 380 nm in a cell was used as an indicator of the free calcium in its cytosol (see Fig. 6 A). The ratios were converted to intracellular calcium concentrations by applying the Grynkiewicz equation, as described previously (29).

Comparison between video microscopy and line scanning

Deflections for a single post were measured by both video microscopy and line scanning for a paired comparison of the two techniques. Measurements were made on the same post, but for different twitch contractions because it was not possible to perform both approaches simultaneously. To assess the variability in maximum force and maximum velocity between twitch contractions, measurements were acquired an individual post for 90 twitch contractions that occurred over 180 s ($n = 6$ cells). The results indicated that twitch-to-twitch variances for a cell were small: $6.7 \pm 2.0\%$ for maximum force and $6.6 \pm 2.0\%$ for maximum velocity. The small variations suggested that a direct comparison could be made between the two techniques, even though the comparison would be made on measurements of different twitch contractions.

Immunofluorescence analysis

To assess myofibril structures, cells were treated with 0.5% Triton X-100 in an ice bath with protease inhibitors (20 μg/mL aprotinin, 1 μg/mL leupeptin, and 1 μg/mL pepstatin from G-Biosciences/Genotech, Maryland Heights, MO), fixed in 4% paraformaldehyde, and blocked with 10% goat serum. Z-bands were stained by incubating cells with monoclonal mouse antibodies against sarcomeric α-actinin (Sigma-Aldrich) and Alexa-Fluor 647 goat anti-mouse IgG antibodies (Invitrogen, Carlsbad, CA). Nuclear staining was conducted using Hoescht 33342 (Invitrogen). Image analysis of circularity in cell shape, sarcomere length, and Z-band width was performed with NIS-Elements software (http://www.nis-elements.com/). Circularity was determined by calculating the spread area of a cell, multiplying by 4π, and dividing by the square of its perimeter, as similar to previous studies (12). Sarcomere length was quantified by drawing an analysis line between two Z-bands and calculating the distance between the peaks in the fluorescence intensities. Z-band width was quantified by applying an edge-detection algorithm to segment the individual bands and then measuring their end-to-end length. At least 10 cells were analyzed per condition.

Statistical analysis

Statistical differences between the four groups of stiffness tested were determined by applying an analysis of variance (ANOVA) with Tukey's post-hoc analysis. A p-value <0.05 were used to determine significance and all data are reported as the average and plus or minus the 95% confidence intervals, unless otherwise specified.

RESULTS

Force and work increase with stiffness

To characterize twitch contractions, arrays of micropost were used as culture substrates for neonatal rat cardiomyocytes. These cells began to spontaneously beat after two days of culture on the arrays, but for each measurement, contractions were stimulated using an applied electric field. Twitch forces were separated into two groupings of posts

based upon their spatial location: 1), those at the perimeter and 2), those within the interior of the cells (Fig. 1 A).

The largest twitch forces were measured at the perimeter and had orientations that were directed centripetally (Fig. 1 B). Twitch forces at the perimeter were determined to be significantly greater than those in the interior (Wilcoxon rank-sum test, $p < 0.05$). Furthermore, the average twitch force per post at the perimeter was twofold larger than those within the interior. Because the perimeter twitch forces were largest, we focused our power analysis on these posts.

Immunofluorescent staining of α-actinin and actin revealed the presence of myofibrils with regular sarcomeric patterns. The α-actinin staining highlighted regular striations that were indicative of sarcomeres (Fig. 1 C), whereas
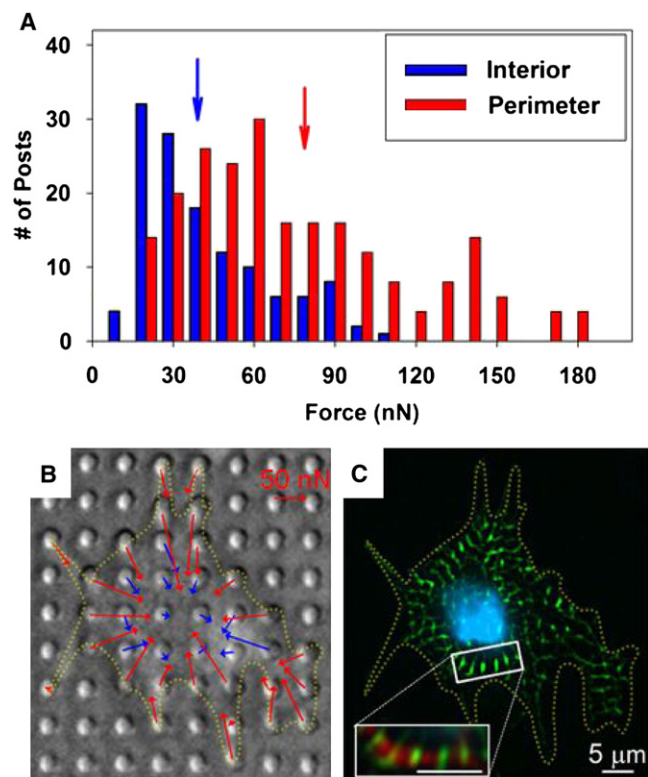

FIGURE 1 Twitch force measurements of neonatal rat cardiomyocytes on microposts. (A) Histogram of the twitch forces shows that forces are larger at the perimeter of the cell in comparison to those at the interior ($E_{eff} = 15$ kPa, $n = 9$ cells, Wilcoxon rank test, $p < 0.05$). The average force per posts at the interior was 38 ± 6 nN (blue arrow), which was significantly less than the force at the perimeter (77 ± 9 nN, red arrow, $p < 0.05$). (B) Force exerted by a cell is measured by the deflection of the post tips ($E_{eff} = 10$ kPa) with phase microscopy. Force vectors at the posts along the perimeter of the cell (red) and in its interior (blue) are overlaid on the phase image of a cell at its maximally contracted state (outlined in yellow). (C) An image of the same cell after it was fixed and stained for sarcomeric α-actinin (green) and its nucleus (cyan). A top-hat transform was applied to the α-actinin image to highlight the Z-bands. (C, inset) A subsection of the cell (outlined in white box) shows the presence of both actin filaments (red) and α-actinin (green) in a regular pattern along a myofibril. Scale bar, 5 μm.

costaining with phalloidin showed the greatest actin concentration within the spacing between the striations (Fig. 1 *C*, *inset*). This regular arrangement of α-actinin and actin denoted the myofibrils expected for a muscle cell. The orientation and development of these myofibrils were a product of the cells adapting to their new environment as described previously (22). Taken together with the deflection measurements of the posts, we could surmise that the forces measured at the posts on the perimeter are associated with myofibril structures developed in vitro.

To assess the effect of stiffness on cardiomyocyte contractility, cells were cultured on arrays of posts with different effective shear moduli (see Appendix). Twitch forces were calculated at individual posts along the perimeter of the cell and averaged for each array. We found a statistically significant correlation between twitch force and stiffness (Fig. 2 *A*; ANOVA, $p < 0.05$). Additionally, forces applied to the posts between twitch contractions, i.e., forces produced during the resting state, increased with stiffness as well (Fig. 2 *A*, ANOVA, $p < 0.05$). By adding the twitch forces and resting forces together, the resulting total force produced by cardiomyocytes was seen to increase from 20 nN for cells on the softest arrays to 120 nN for those on the stiffest arrays. The increase in twitch force also corresponded with an increase in the contractile work of the cells (Fig. 2 *B*). Others have observed similar results in force and work in response to substrate stiffness (12,15,16,30), but measuring the twitch force using microposts allowed us to directly link the effect of stiffness to the myofibrils associated at the posts. Thus, these results indicated that cardiomyocytes cultured on stiffer substrates can produce greater force and work with their subcellular arrangement of myofibrils.
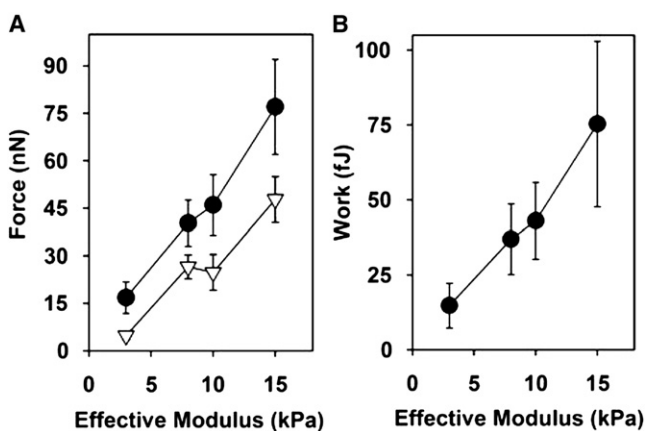
Temporal resolution critical for measuring twitch velocity

To gain insights into how twitch dynamics change with stiffness, we developed a force analysis approach with an improved rate of data sampling. Specifically, a line scanning approach was used instead of video microscopy to track the deflection of individual posts (Fig. 3 *A*). The necessity for greater temporal resolution was confirmed by comparing the deflections of the same post measured with both approaches (Fig. 3 *B*). The deviation between the two approaches could be observed at the start of the contraction phase, when the twitch velocity accelerates from zero to its maximum velocity. The maximum velocity measured by the two approaches differed on average by 37.9 $\pm$ 17.3% ($n = 10$ posts), which was significantly greater than the twitch-to-twitch variance in the maximum velocity (6.6 $\pm$ 2.0%, in Materials and Methods). Furthermore, the increase in precision was indicated by comparing the 95% confidence intervals for maximum velocity for the two approaches. For line scanning, its confidence interval was
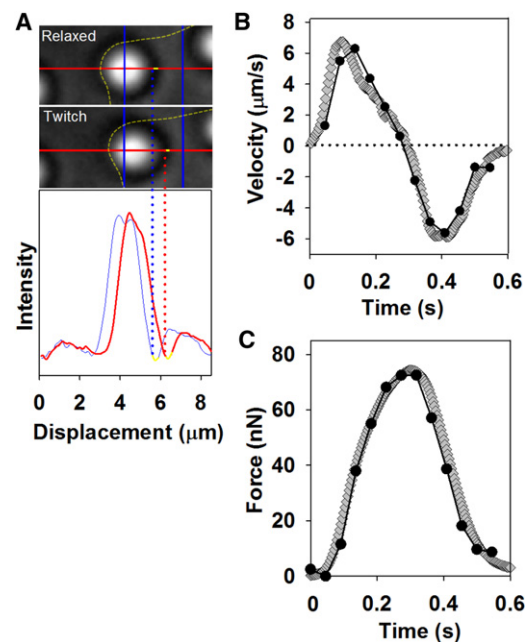

FIGURE 3 Comparison of the temporal resolution for line scanning versus video microscopy. (*A*) Under phase contrast, an analysis line (*red line*) was drawn to overlap with the direction of movement of a micropost by the twitch contraction of a cardiomyocyte. The deflection of the post was tracked from the cardiomyocyte's resting state (*top panel*) to its twitch state (*middle panel*). For the post shown, the intensity profile along the analysis line was plotted (*bottom panel*) for the resting state (*blue curve*) and the twitch state (*red curve*). The deflection of the post was tracked by monitoring the change in the position of its leading edge, which was determined by position of the local minimum (*yellow segment*) in the intensity profile. (*B*) Twitch velocity versus time for twitch contraction at a representative post measured with either line scanning (*gray*) or video microscopy (*black*). (*C*) Twitch force versus time for a representative post measured with either line scanning (*gray*) or video microscopy (*black*).

FIGURE 2 Contractility in cardiomyocytes increases with substrate stiffness. (*A*) Twitch force and (*B*) contractile work at the perimeter of cells increase with the effective shear modulus of the micropost arrays on which they are cultured (*solid circles*). Panel *A* shows the forces measured for cardiomyocytes in the resting state (*open triangles*). All values represent the average per post measured by live cell video microscopy. Error bars represent the 95% confidence intervals.

25% of the mean, whereas for video microscopy it was 38% of the mean. Thus, the increased temporal resolution of line scanning provided more accuracy and precision in measuring twitch velocity.

Twitch force measured by line scanning was determined to be slightly more accurate than video microscopy (Fig. 3 C). Maximum twitch force was measured by both approaches on the same post and found to differ by only 11.2 ± 3.8% ($n = 10$ posts). Again, the increase in data sampling near the point of maximum force by line scanning enables it to provide more accuracy in its measurement. However, because the twitch-to-twitch variance in the maximum force at a post was 6.7 ± 2.0% (in Materials and Methods), both methods were considered reasonable for measuring the maximum twitch force. Thus, the results presented here for absolute force and work can be compared with those reported by others (12,16,30).

Stiffness increases twitch power

To determine the effect of substrate stiffness on twitch power, we cultured cells on post arrays with different effective shear moduli and compared the relationship between force and velocity during twitch contractions. The force-velocity relationships were significantly different for cardiomyocytes cultured on the different post arrays (Fig. 4 A). As observed with video microscopy, maximum twitch force increased for cells on the stiffer posts (Fig. 2 A, ANOVA, $p < 0.001$). However, by using line scanning, maximum twitch velocity was found to decrease with post stiffness (Fig. 4 A, inset, ANOVA, $p < 0.001$). Maximum velocity and its corresponding twitch force at which maximum velocity was reached were compared for cells on arrays of different stiffness and were found to have an inverse relationship expected for muscle (Fig. 4 A, inset, ANOVA, $p < 0.001$) (14,18,21). Thus, these results indicated that higher substrate stiffness can induce cardiomyocytes to modify their contractility by producing faster twitches with less force on the softest substrates, and slower but more forceful twitches on the stiffer substrates.

The effect of higher substrate stiffness on the force-velocity relationship resulted in greater twitch power for the cardiomyocytes. Twitch power was defined as the product of the instantaneous velocity of a cardiomyocyte pulling a post and the resistive load from the springlike behavior of the post (19,21). The resistive load here was not constant throughout a twitch contraction, but increased linearly with the deflection of a post due to its behavior as a Hookean spring. Subsequently, power curves were generated with respect to the resistive load, and maximum twitch power was found to increase with substrate stiffness (Fig. 4 B; ANOVA, $p < 0.001$). Thus, higher stiffness promoted the cells to generate twitch contractions that had more power, leading to improved cardiac contractility.
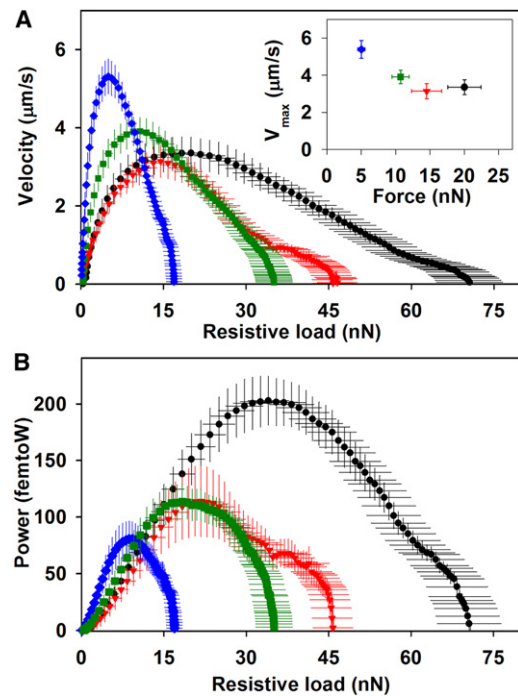

FIGURE 4 Twitch power increases with stiffness. (A) The relationship between twitch force and velocity was plotted for the twitch contraction of cardiomyocytes cultured on arrays with stiffness of 3 kPa (blue diamonds), 8 kPa (green squares), 10 kPa (red triangles), and 15 kPa (black circles). Higher substrate stiffness increased the maximum force reach during a twitch contraction, but also decreased the maximum velocity. (Inset) Maximum velocity versus the instantaneous force at which maximum velocity was reached. (B) Twitch power was plotted as a function of the resistive load and shows that maximum power (denoted by asterisks) increased with substrate stiffness. Error bars represent standard error of the mean.

Myofibril structures are altered with substrate stiffness

To determine whether the change in twitch power could be correlated with biomechanical changes in myofibril structure, images of α-actinin were analyzed to quantify sarcomere length and Z-band width. Cells on either the softest posts (Fig. 5 A) or the stiffest posts (Fig. 5 B) displayed regular striations of α-actinin bands and did not have a significant difference in cell shape. Specifically, circularity in the shape of the cells was not seen to be significantly altered by post stiffness (0.55 ± 0.21 for 9 kPa and 0.52 ± 0.09 for 15 kPa), which is similar to observations made previously (12,16). Quantifying the spacing between bands and the length of bands provided an indication of sarcomere length and Z-band width, respectively. Sarcomere length is associated with the degree of thick and thin filament overlap, which affects the probability of actin-myosin cross-bridge formation and thus the capacity to generate force (14,19,20). Here, sarcomere length increased significantly with stiffness from 1.76 ± 0.06 μm on the softest posts to 1.95 ± 0.06 μm on the stiffest post (Fig. 5 C, ANOVA, $p < 0.001$). These sarcomere lengths were within
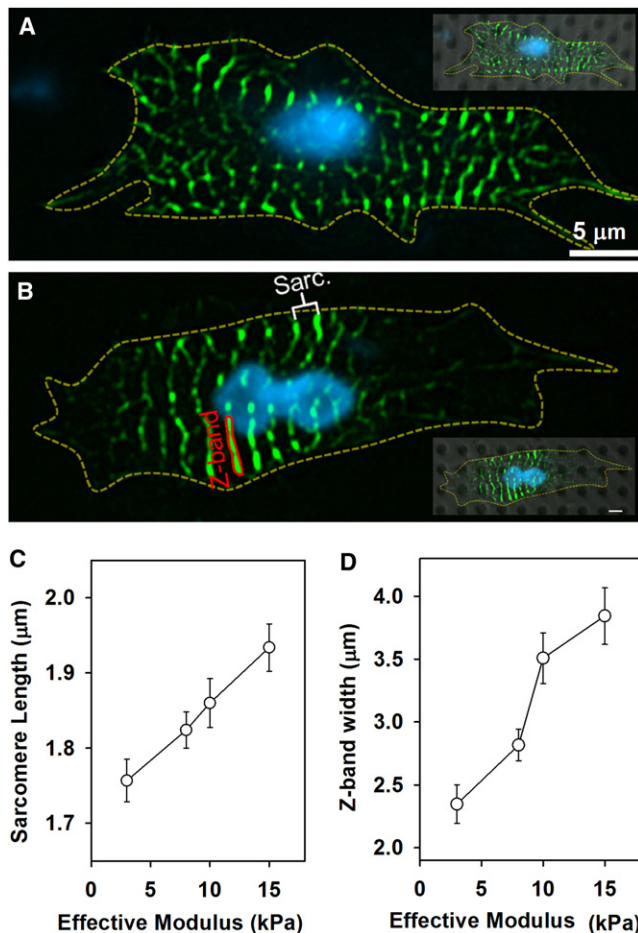
FIGURE 5   Resting sarcomere length and Z-band width increase with stiffness. Cells on the (*A*) softest arrays (3 kPa) and on the (*B*) stiffest arrays (15 kPa) were fixed and stained for α-actinin (*green*) and nuclei (*blue*). (*Insets*) Same cell with a bright-field image showing the microposts. (*C*) Sarcomere length and (*D*) Z-band width increased with substrate stiffness (ANOVA *p* < 0.001). Error bars represent the 95% confidence intervals. Scale bars, 5 μm.

the working range for cardiac muscle observed previously (20). On the other hand, Z-band widths are associated with increased uniformity and synchronicity of a contraction because they maintain the alignment of parallel myofibrils and hold adjacent sarcomeres in register during a twitch contraction (31). Similar to sarcomere length, Z-band width improved significantly with stiffness, increasing from 2.35 ± 0.30 μm for cells on the softest post to 3.84 ± 0.40 μm for those on the stiffest post (Fig. 5 *D*, *p* < 0.001 ANOVA). Taken together, these results indicate that culturing cardiomyocytes on stiffer substrates led to a myofibril structure that helped to improve cardiac contractility.

Intracellular calcium levels are higher on stiffer posts

To determine whether the effect of stiffness can also be attributed to biochemical changes in intracellular calcium,

ratiometric fluorescent intensity of Fura-2 in cardiomyocytes was monitored throughout the twitch contractions. Basal levels (resting state), maximum calcium concentrations, and the amplitude of the calcium transient during a contraction were significantly larger for cells on the stiffer posts as compared to those on the softer posts (Fig. 6 *A*). Similar to our observations, the amplitude of the calcium transient has been observed to increase with stiffness for neonatal rat cardiomyocytes cultured on polyacrylamide gels (12). The increase in the basal calcium with stiffness likely corresponded in part to an increase in forces during the resting state (Fig. 2 *A*). Likewise, the increase in the maximum calcium concentration and transient amplitude with stiffness can be correlated with the increase in their twitch forces (Fig. 2 *A*). Thus, higher stiffness leads to changes in calcium concentrations that produce greater forces at the resting state and during twitch contractions.

An advantage of our approach is that the dynamics in calcium and twitch contraction can be compared directly. Simultaneous measurements of force and calcium were conducted for cells on arrays of either low (Fig. 6 *B*) or high
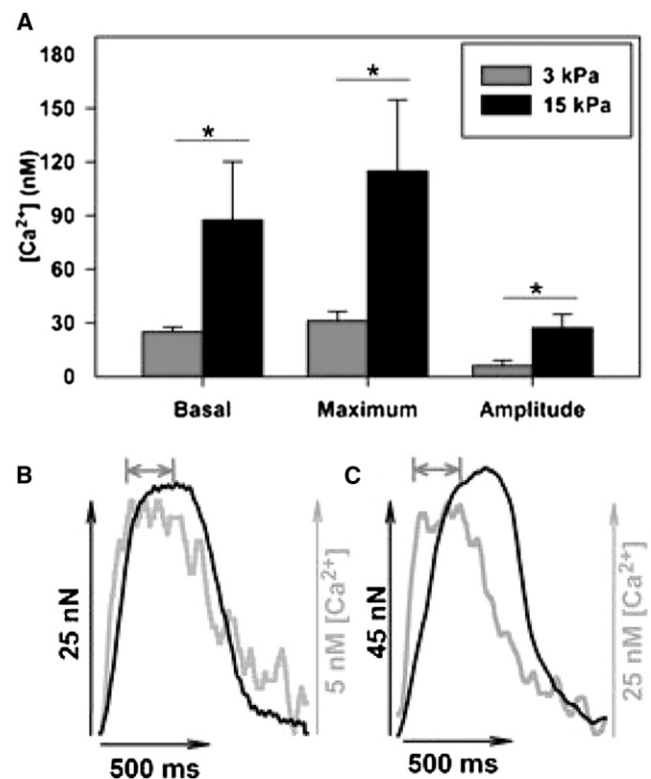
FIGURE 6   Intracellular calcium increases with substrate stiffness. (*A*) Basal levels, maximum calcium concentration, and the amplitude of the rise in calcium for a twitch contraction increase with substrate stiffness (*shaded*, 3 kPa; *solid*, 15 kPa). (*Asterisk*) *p* < 0.05 tested between stiffnesses. Examples of corresponding traces for calcium (*shaded*) and force (*solid*) for cardiomyocytes on (*B*) 3 kPa and (*C*) 15 kPa arrays of posts. The duration of the steady-state concentration in intracellular calcium (*shaded bar*, 120 ms) was defined by the time calcium levels remained >90% of the maximum concentration.

(Fig. 6 C) stiffness. For both arrays, calcium concentrations were observed to have a quasi-steady-state behavior at maximum calcium (denoted by the *bar* above each calcium trace in Fig. 6, *B* and *C*). However, higher substrate stiffness led to a longer duration of this quasi-steady state, indicating that stiffness can increase the duration of maximum calcium ($\Delta t_{Ca,90}$ in Table 1). A similar quasi-steady state in the calcium transient has been observed previously for neonatal cardiomyocyte and has been proposed to result from an underdeveloped sarcoplasmic reticulum (32,33). In addition, comparing the temporal measurements of force and calcium revealed that the time to maximum calcium ($t_{Ca,90}$) was reached before maximum force (t_{90}), which is typical for a twitch contraction in muscle (Table 1). Moreover, the time to maximum velocity (t_{Vmax}) coincided with maximum calcium, but only for cells on the stiffest arrays (Table 1). For cells on the softest arrays, maximum twitch velocity was reached before maximum calcium (Table 1), after which twitch velocity reduced to $57 \pm 12\%$ of its maximum at same the time that maximum calcium was reached (data not shown). Taken together, these results indicate that maximum velocity is not limited by the maximum calcium concentration on the softest posts, which suggests stiffness effects cannot be accounted for by changes in calcium concentration alone.

DISCUSSION

The major conclusions from this study on the contractile power of neonatal cardiomyocytes are that 1), line scanning with microposts can increase the measurement accuracy for both twitch velocity and force; 2), cardiomyocyte increase their twitch power in response to higher substrate stiffness; and 3), this increase in twitch power is correlated with changes in the structure of the sarcomeres and increased intracellular calcium levels.

Subcellular dynamics as a metric of development

Arrays of microposts were used to quantify twitch forces at individual points of adhesion, which provided subcellular measurements of cardiac contractility. These subcellular measurements can more directly assess the contractile nature of the myofibrils, which in turn, can offset the

morphological differences between neonatal and adult cardiomyocyte (7,8). Adult cardiomyocytes in vitro maintain their cylindrical morphology found in vivo, whereas neonatal cardiomyocytes flatten and spread in all directions, which complicates direct comparisons between the two. On micropost arrays, neonatal cardiomyocytes still flatten and spread, but the adhesion formed at the tip of a post is associated with one-to-several myofibrils (Fig. 1 *A*). Thus, measurements of twitch force, velocity, and power using microposts can be correlated with the contraction of myofibrils in a manner than is independent of cell shape.

In comparing twitch force and twitch velocity measured for cardiomyocytes on the stiffest posts, our results suggests that the contraction of myofibrils in neonatal cardiomyocyte is similar to those in adults. Specifically, it is estimated from isolated myofibril measurements that adult myofibrils produce ~71 nN of force during a twitch at submaximal calcium (18,34). Similarly, we observed on average of 77 nN of force per post for neonatal cells on the stiffest substrates (Fig. 2 *A*). However, maximum velocity of shortening was an order-of-magnitude slower for neonatal cardiomyocytes on the stiffest substrates (3.3 μm/s; Fig. 4 *A*) as compared to adults measured under a similar resistive load (38 μm/s (18)). This lower velocity in neonatal cardiomyocytes resulted in a twitch power per myofibril that was lower than in adults. Specifically, an adult cardiomyocyte can generate 25 pW of power, which is produced by 40–50 parallel myofibrils contracting with the same velocity (18). Therefore, we can estimate that a single adult myofibril generates, on average, between 500 and 625 fW of power, which is threefold more than the 203 fW per post measured for neonatal cardiomyocytes on the stiffest arrays (Fig. 4 *B*). As a consequence, twitch power could be a better metric to resolve the differences in the contractile developmental of myofibrils between adult and neonatal stages.

Myofibril and calcium changes yield increased twitch power

The increased twitch power on stiffer posts can be attributed in part to the changes in the myofibril structure of neonatal cardiomyocytes. Here, one would expect an increase in power to develop from hypertrophic growth cues in the environment, e.g., post stiffness (15). Hypertrophy leads to

TABLE 1 Temporal parameters of the twitch contraction on each stiffness

E_{eff} (kPa)	k_{post} (nN/μm)	n_{post} [n_{cell}]	t_{90} (ms)*	t_{Vmax} (ms)*	$t_{ca,90}$ (ms)*	$\Delta t_{ca,90}$ (ms)
3 ± 2	29 ± 14	63 [21]	208 ± 18	59 ± 6	100 ± 16	101 ± 16
8 ± 1	76 ± 8	62 [15]	212 ± 12	64 ± 4	-	-
10 ± 1	103 ± 14	49 [15]	236 ± 20	75 ± 10	-	-
15 ± 2	142 ± 30	63 [20]	252 ± 18	87 ± 16	83 ± 12	124 ± 18

Values are means $\pm 95\%$ confidence interval. Parameters: E_{eff}, substrate effective shear modulus; k_{post}, post spring constant; n_{post}, number of posts; n_{cell}, number of cells; t_{90}, time to 90% force; t_{Vmax}, time to maximum velocity; $t_{ca,90}$, time to 90% calcium; $\Delta t_{ca,90}$, duration of time calcium was >90% ($n = 17$ for 3 kPa and 10 for 15 kPa).
*Difference within the group at $p < 0.005$.

myofibrils with more contractile protein content and/or increased number of myofibrils at points of adhesion (4,5). However, previous studies have suggested that higher stiffness does not significantly affect the concentration of sarcomeric proteins or their isoform expression (12,16). Our analysis of the myofibril structure revealed sarcomeres had increased resting length as well as a greater degree of coupling at their Z-disk with increasing post stiffness, both of which are linked to improved contractility (Fig. 5, C and D). Assuming that thick and thin filament lengths are not altered (not measured in this study), the increased resting sarcomere length from 1.76 μm to 1.95 μm suggests that during a contraction, there is a greater change in length of the overlap between these filaments. Subsequently, longer sarcomeres should increase the number of binding events for actin-myosin cross-bridges, which could at least partially explain the increase in twitch force and power observed with higher substrate stiffness (20). Additionally, increased myofibril coupling likely maintains uniformity in sarcomere length across the structural array by holding the Z-disks in register through the lateral transmission of forces between parallel myofibrils (31). The importance of this is demonstrated by several subcellular events that can lead to sarcomeric disarray and myofibril misalignment, such as 1), spontaneous oscillatory contraction events (35); 2), nonhomogeneous rising phase of calcium (32,33); and 3), random sarcomeric yielding in response to increased stress (35). Higher resistive load could potentially induce misalignment of myofibrils if not coupled. Maintaining sarcomeres in register can also synchronize myofibril contraction to produce a faster twitch velocity. Even though maximum velocity decreased with stiffness, cardiomyocytes on the stiffest posts contracted longer (Table 1) and at higher loads relative to cells on the softer substrates resulting in greater twitch power (Fig. 4 A). Thus, increased resting sarcomere length and the degree of myofibril coupling are structural modifications that may explain greater twitch power on stiffer substrates.

An increase in the intracellular calcium concentration with stiffness likely contributed to an increase in maximal twitch force, but calcium was seen to have a limited role in twitch dynamics on the softest posts. The larger baseline and peak calcium concentrations on the stiffest posts (Fig. 6 A) corresponded with increased resting and maximum twitch force (Fig. 2 A). Previous studies have demonstrated an increase in sarco/endoplasmic reticulum calcium ATPase expression with stiffness (12), which could explain the increase in calcium concentration during twitches on stiffer posts (36). Increased intracellular calcium should increase the activation of thin filaments, resulting in more actin-myosin cross-bridges, and therefore more force and velocity per myofibril (13,14). Contrary to these observations, however, maximum velocity was highest on the softest posts despite the lower levels of calcium. The lower resistive load at the softest posts likely permitted a faster contraction

with less calcium, but differences in the mechanical properties of the posts cannot account for the altered temporal relationship between calcium and velocity observed on the softest posts (Fig. 6, B and C, and Table 1). If the concentration of intracellular calcium was the primary factor in determining twitch velocity, maximum velocity on the softest posts should have increased in tandem with calcium levels and not preceded maximum calcium as we observed. Therefore, it is plausible that differences in myofibril structure associated with different post stiffness can affect twitch velocity as well.

CONCLUSION

We have developed what consider a novel in vitro approach with sufficient temporal resolution to measure twitch force and twitch velocity, allowing us to determine that twitch power is sensitive to substrate stiffness for neonatal rat cardiomyocytes. The increase in twitch power with higher substrate stiffness is correlated with modifications of myofibril structure and intracellular calcium that work synergistically to improve the number of actin-myosin cross-bridges. The effects of stiffness on twitch power suggest it may play a role in the transition of neonatal cardiomyocytes to the more adult phenotype during development. However, the large difference that exists between twitch power for neonatal cardiomyocytes in this study and that of the adult stage suggests that stiffness is only one of several factors that play a role in the development of contractility.

APPENDIX: DERIVATION OF EFFECTIVE SHEAR MODULUS FOR POST ARRAYS

Studies using elastomeric post arrays have reported the spring constant of the posts as a way to evaluate the stiffness of a substrate (37). The spring constant is an appropriate measure for the stiffness of an individual post (usually having units of nN/μm), but it does not represent the compliance of the overall array of posts underneath a cell. Here, the concept of effective shear modulus is presented to describe the substrate stiffness of the post arrays.

The effective shear modulus (having units of N/m^2 or Pa) is found by assuming that an array of discrete posts underneath a cell can be regarded as a continuum. A force P acting on an individual post can be equated to a transverse stress τ_{xz} acting on the representative volume element (RVE) at its top surface (Fig. 7). It can also be assumed that there is a fixed boundary condition at the base of a post, which allows the post to deflect as a cantilever beam.

For the coordinate system shown, let x, y, and z be the coordinate directions and u, v, and w be deformations of the RVE in the x, y, and z directions, respectively. The deformed state of the RVE can be regarded as a case of simple shear in the x direction. The shear modulus of the RVE in the x direction on its top plane, whose normal is in the z direction, is given by

$$G_{xz} = \frac{\tau_{xz}}{2\varepsilon_{xz}}, \qquad (7)$$

where ε_{xz} is the shear strain in the x direction on the top plane. Because the transverse stress is assumed to be uniformly distributed and thus is
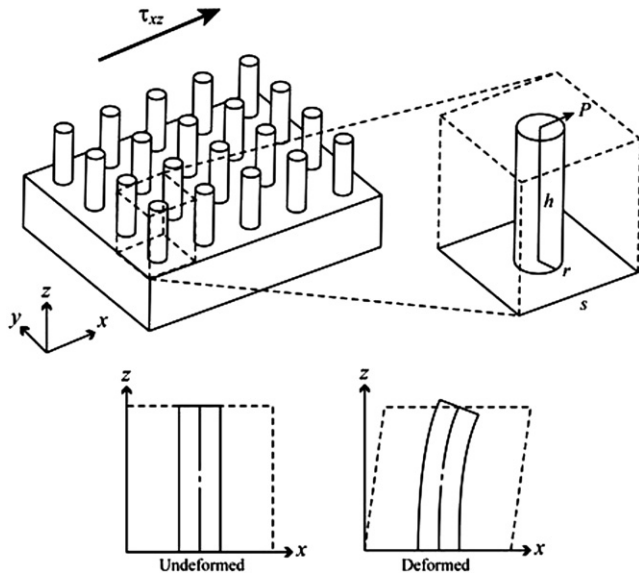
FIGURE 7 Schematic of a transverse stress τ_{xz} acting on the surface of the array of posts in the x direction. The representative volume element (RVE) is bounded by height h and area s^2 and contains a single post with radius r. The transverse stress τ_{xz} is assumed to be uniformly distributed across the top surface of the RVE and is equal to a force P acting on the post divided by the area of the top surface s^2. The force P acts in the same direction as τ_{xz}. Two-dimensional schematics of the RVE are shown in the undeformed and deformed states.

equivalent to a force P acting on the unit volume divided by the area of top surface, it can be expressed as

$$\tau_{xz} = \frac{P}{s^2}. \tag{8}$$

Likewise, the shear strain ε_{xz} is a component of Green's strain tensor and is

$$\varepsilon_{xz} = \frac{1}{2}\left(\frac{\partial u}{\partial z} + \frac{\partial w}{\partial x} + \frac{\partial u}{\partial x}\frac{\partial u}{\partial z} + \frac{\partial v}{\partial x}\frac{\partial v}{\partial z} + \frac{\partial w}{\partial x}\frac{\partial w}{\partial z}\right). \tag{9}$$

It is important to note that for small displacements, the quadratic terms can be neglected. However, if these terms are retained for a deformation of the RVE that is not small, then for a case of simple shear, displacement in the y direction and the derivatives of the displacements for all but $\partial u/\partial z$ are zero ($v = 0$, $\partial u/\partial x = \partial w/\partial x = \partial w/\partial z = 0$). Thus, this equation reduces to

$$\varepsilon_{xz} = \frac{1}{2}\frac{\partial u}{\partial z}. \tag{10}$$

The shear strain of the RVE is given by considering the defection of the post, which defines the deformed state of RVE. According to Euler-Bernoulli beam theory, the displacement of a cantilever u can be derived from equation of the elastic curve as

$$u(z) = \frac{Pz^2}{6E_{pdms}I_z}(3h - z), \tag{11}$$

where E_{pdms} is the elastic modulus of PDMS, I_z is the second moment of area about the z axis, which for a cylindrical post is $I_z = \pi\, r^4/4$, and h is the height of a post. From Eq. 10, the shear strain ε_{xz} can be calculated as

$$\varepsilon_{xz} = \frac{1}{2}\frac{\partial u}{\partial z} = \frac{\partial}{\partial z}\left(\frac{Pz^2}{12E_{pdms}I_z}(3h - z)\right)\bigg|_{z=h} = \frac{Ph^2}{4E_{pdms}I_z}. \tag{12}$$

Substituting for I_z and P yields

$$\varepsilon_{xz} = \frac{\tau_{xy}s^2h^2}{\pi E_{pdms}r^4}. \tag{13}$$

Hence, substituting ε_{xz} into Eq. 7 produces

$$G_{xz} = \frac{\pi}{2}\frac{E_{pdms}r^4}{s^2h^2}. \tag{14}$$

From this relationship, the effective shear modulus of the RVE increases with a radius of a post to the fourth order, whereas it decreases with s and h to the second order.

REFERENCES

1. Jacot, J. G., J. C. Martin, and D. L. Hunt. 2010. Mechanobiology of cardiomyocyte development. *J. Biomech.* 43:93–98.

2. Prakash, Y. S., M. J. Cody, …, G. C. Sieck. 1999. Comparison of cross-bridge cycling kinetics in neonatal vs. adult rat ventricular muscle. *J. Muscle Res. Cell Motil.* 20:717–723.

3. Hopkins, Jr., S. F., E. P. McCutcheon, and D. R. Wekstein. 1973. Postnatal changes in rat ventricular function. *Circ. Res.* 32:685–691.

4. Rudolph, A. M., and M. A. Heyman. 1974. Fetal and neonatal circulation and respiration. *Annu. Rev. Physiol.* 36:187–207.

5. Wu, Y., and E. X. Wu. 2009. MR study of postnatal development of myocardial structure and left ventricular function. *J. Magn. Reson. Imaging.* 30:47–53.

6. Nassar, R., M. C. Reedy, and P. A. Anderson. 1987. Developmental changes in the ultrastructure and sarcomere shortening of the isolated rabbit ventricular myocyte. *Circ. Res.* 61:465–483.

7. Claycomb, W. C. 1977. Cardiac-muscle hypertrophy. Differentiation and growth of the heart cell during development. *Biochem. J.* 168:599–601.

8. Goss, R. J. 1966. Hypertrophy versus hyperplasia. *Science.* 153:1615–1620.

9. Gilbert, P. M., K. L. Havenstrite, …, H. M. Blau. 2010. Substrate elasticity regulates skeletal muscle stem cell self-renewal in culture. *Science.* 329:1078–1081.

10. Zemel, A., F. Rehfeldt, …, S. A. Safran. 2010. Optimal matrix rigidity for stress fiber polarization in stem cells. *Nat. Phys.* 6:468–473.

11. Forte, G., F. Carotenuto, …, P. Di Nardo. 2008. Criticality of the biological and physical stimuli array inducing resident cardiac stem cell determination. *Stem Cells.* 26:2093–2103.

12. Jacot, J. G., A. D. McCulloch, and J. H. Omens. 2008. Substrate stiffness affects the functional maturation of neonatal rat ventricular myocytes. *Biophys. J.* 95:3479–3487.

13. McDonald, K. S., L. J. Field, …, R. L. Moss. 1995. Length dependence of Ca^{2+} sensitivity of tension in mouse cardiac myocytes expressing skeletal troponin C. *J. Physiol.* 483:131–139.

14. Sonnenblick, E. H. 1962. Force-velocity relations in mammalian heart muscle. *Am. J. Physiol.* 202:931–939.

15. Lammerding, J., R. D. Kamm, and R. T. Lee. 2006. Mechanotransduction in cardiac myocytes. *Ann. NY Acad. Sci.* 1015:53–70.

16. Engler, A. J., C. Carag-Krieger, …, D. E. Discher. 2008. Embryonic cardiomyocytes beat best on a matrix with heart-like elasticity: scar-like rigidity inhibits beating. *J. Cell Sci.* 121:3794–3802.

17. Jacot, J. G., H. Kita-Matsuo, …, A. D. McCulloch. 2010. Cardiac myocyte force development during differentiation and maturation. *Ann. N. Y. Acad. Sci.* 1188:121–127.

18. Korte, F. S., and K. S. McDonald. 2007. Sarcomere length dependence of rat skinned cardiac myocyte mechanical properties: dependence on myosin heavy chain. *J. Physiol.* 581:725–739.

19. Woledge, R. C., N. A. Curtin, and E. Homsher. 1985. Energetic aspects of muscle contraction. *Monogr. Physiol. Soc.* 41:1–357.

20. Gordon, A. M., E. Homsher, and M. Regnier. 2000. Regulation of contraction in striated muscle. *Physiol. Rev.* 80:853–924.

21. Hill, A. V. 1938. The heat of shortening and the dynamic constants of muscle. *Proc. R. Soc. Lond. B Biol. Sci.* 126:136–195.

22. Zhao, Y., and X. Zhang. 2007. Adaptation of myofibrils to a microstructured polymeric substrate. *Sens. Actuators A Phys.* 136:491–495.

23. Zhao, Y., and X. Zhang. 2006. Cellular mechanics study in cardiac myocytes using PDMS pillars array. *Sens. Actuators A Phys.* 125:398–404.

24. Kim, K., R. Taylor, …, B. L. Pruitt. 2011. Calibrated micropost arrays for biomechanical characterization of cardiomyocytes. *Micro Nano Lett.* 6:317–322.

25. Sniadecki, N. J., and C. S. Chen. 2007. Microfabricated silicone elastomeric post arrays for measuring traction forces of adherent cells. *Methods Cell Biol.* 83:313–328.

26. Liang, X. M., S. J. Han, …, N. J. Sniadecki. 2010. Platelet retraction force measurements using flexible post force sensors. *Lab Chip.* 10:991–998.

27. Moreno-Gonzalez, A., F. S. Korte, …, M. Regnier. 2009. Cell therapy enhances function of remote non-infarcted myocardium. *J. Mol. Cell. Cardiol.* 47:603–613.

28. Sniadecki, N. J., C. M. Lamb, …, D. H. Reich. 2008. Magnetic microposts for mechanical stimulation of biological cells: fabrication, characterization, and analysis. *Rev. Sci. Instrum.* 79:044302.

29. Grynkiewicz, G., M. Poenie, and R. Y. Tsien. 1985. A new generation of Ca^{2+} indicators with greatly improved fluorescence properties. *J. Biol. Chem.* 260:3440–3450.

30. Kajzar, A., C. M. Cesa, …, R. Merkel. 2008. Toward physiological conditions for cell analyses: forces of heart muscle cells suspended between elastic micropillars. *Biophys. J.* 94:1854–1866.

31. Campbell, K. S. 2009. Interactions between connected half-sarcomeres produce emergent mechanical behavior in a mathematical model of muscle. *PLOS Comput. Biol.* 5:e1000560.

32. Escobar, A. L., R. Ribeiro-Costa, …, R. Mejía-Alvarez. 2004. Developmental changes of intracellular Ca^{2+} transients in beating rat hearts. *Am. J. Physiol. Heart Circ. Physiol.* 286:H971–H978.

33. Korhonen, T., S. L. Hänninen, and P. Tavi. 2009. Model of excitation-contraction coupling of rat neonatal ventricular myocytes. *Biophys. J.* 96:1189–1209.

34. Stehle, R., J. Solzin, …, C. Poggesi. 2009. Insights into the kinetics of Ca^{2+}-regulated contraction and relaxation from myofibril studies. *Pflugers Arch.* 458:337–357.

35. Shimamoto, Y., M. Suzuki, …, S. Ishiwata. 2009. Inter-sarcomere coordination in muscle revealed through individual sarcomere response to quick stretch. *Proc. Natl. Acad. Sci. USA.* 106:11954–11959.

36. Stokke, M. K., K. Hougen, …, A. W. Trafford. 2010. Reduced SERCA2 abundance decreases the propensity for Ca^{2+} wave development in ventricular myocytes. *Cardiovasc. Res.* 86:63–71.

37. Saez, A., A. Buguin, …, B. Ladoux. 2005. Is the mechanical activity of epithelial cells controlled by deformations or forces? *Biophys. J.* 89:L52–L54.